

# An ultrahigh-density digital data read-out method based on grazing-angle incidence x-ray backscattering diffraction

Hakob (Akop) P Bezirganyan<sup>1</sup>, Hayk H Bezirganyan Jr<sup>2</sup>,  
Siranush E Bezirganyan<sup>3</sup>, Petros H Bezirganyan Jr<sup>4</sup> and  
Youri G Mossikyan<sup>5</sup>

<sup>1</sup> Department of Solid State Physics, Yerevan State University, #1, Alex Manoogian Street, Yerevan City, AM 375025, Republic of Armenia

<sup>2</sup> Department of Informatics and Applied Mathematics, Yerevan State University, #1, Alex Manoogian Street, Yerevan City, AM 375025, Republic of Armenia

<sup>3</sup> Department of Medical and Biological Physics, Yerevan State Medical University after Mkhitar Heratsi, #2, Koryun Street, Yerevan City, AM 375025, Republic of Armenia

<sup>4</sup> Department of Computer Science, State Engineering University of Armenia, #105, Terian Street, Yerevan City, AM 375009, Republic of Armenia

<sup>5</sup> Yerevan Automated Control Systems Computer Scientific-Research Institute, #3, H Hakobyan Street, Yerevan City, AM 375033, Republic of Armenia

E-mail: [hakob\\_bezirganyan@yahoo.co.uk](mailto:hakob_bezirganyan@yahoo.co.uk)

Received 22 February 2005, accepted for publication 8 August 2005

Published 12 September 2005

Online at [stacks.iop.org/JOptA/7/604](http://stacks.iop.org/JOptA/7/604)

## Abstract

An ultrahigh-density x-ray optical data storage medium useful for terabyte-scale memory applications and named X-ROM is proposed. The X-ROM is a nanocrystalline semiconductor layer, in which non-diffracting nanosized reflectors of x-radiation are embedded. The procedure of digital data read-out from the X-ROM can be performed e.g. by the application of a grazing-angle incidence x-ray backscattering diffraction technique under conditions of specular vacuum wave suppression. The surface storage digital data density of the proposed device, with 20 nm/bit linear size of the single-bit domain, is higher by two orders of magnitude than the volumetric data density actually achieved for a three-dimensional optical data storage medium.

**Keywords:** data read-out, zone-plate-array lithography, grazing-angle incidence x-ray, crystalline layer, backscattering diffraction, specular beam suppression, Mathieu functions

## 1. Introduction

The history of information technology has been a history of miniaturization of the 'bits', i.e. a tendency towards supplying data storage systems based on ultrahigh-density information carriers with long-term stability, this storage capacity having become equivalent to the information in large libraries. Optical data storage is very convenient for use due to storage media being removable. Read-only memory (ROM) is a read-only optical data storage medium, where the data are recorded during the manufacture

of the disks. ROM systems detect the stored data by sensing changes in the intensity or polarization of a reflected laser beam as the focused spot scans along a data track. In the form of the compact disk (CD), this optical data storage medium is used widely for music distribution and for computer software (CD-ROM). In this case the data read-out procedure retrieves data by sensing changes in reflectivity of the patterned, metallized film deposited on a plastic substrate. The digital video disk (DVD) standard offers higher area density per layer, and as many as four layers of recorded information with sufficient read-out bandwidth and

capacity for distribution of several hours' worth of high-quality compressed video.

In the read–write media optical disks a laser beam is used to write and read a bit of information. Like the read-only optical CDs, they can be removed or inserted by the user. The bit size scales with the wavelength of light, although some schemes enable one to exceed this limit. In phase-change media, a suitably intense laser beam crystallizes an amorphous film. A higher-intensity laser beam reverses the crystallization by melting the material, which then cools back to the amorphous phase. Information is read by measuring the reflectivity of the film since the optical reflectivity of the crystalline phase is different from that of the amorphous phase.

Recently an ultrahigh-density ferroelectric data recording system based on purely electrical principles using a scanning non-linear dielectric microscopy technique and ferroelectric thin films of LiTaO<sub>3</sub> single crystals was developed (see [1]). A nanosized domain dot array of areal density 1.50 terabit per square inch has been successfully demonstrated in a surface of a LiTaO<sub>3</sub> single-crystal film. The radius of the domain dots was 10.4 nm. These nanodots remained stable at least over 24 h, and could be overwritten with dots.

Ultrahigh-density x-ray optical memory, named X-ROM, which is useful for terabyte-scale digital data storage applications, is proposed in this paper, as well as in the papers [2, 3]. Such wavelength consideration is stipulated for the following reasons. Contemporary information nanotechnological processes require non-destructive methods for sample characterization. First of all, X-ROM is an ultrahigh-density information carrier with long-term stability because the x-ray diffraction methods are non-destructive compared with other local probing approaches such as transmission electron microscopy (TEM), scanning electron microscopy (SEM) and more recently scanning tunnelling microscopy (STM) and atomic force microscopy (AFM). The application of these imaging techniques with atomic resolution has become a standard in the most advanced laboratories. However, every technique has its limitations: for example SEM, AFM and STM can only be used to visualize surfaces, while the analysis with the TEM is destructive and requires very thin samples and complex preparation procedures. Moreover, all microscopy techniques involving electrons or other charged particles for sample probing need vacuum conditions. These limitations are usually not encountered with x-rays (and in particular 'hard' x-rays, i.e. with energies from a few keV to few tens of keV), which can penetrate deeply into condensed matter and are not absorbed in air, permitting one to investigate the sample in its natural environment at atmospheric pressure (e.g. see [4–8]). Different x-ray scattering and diffraction techniques can provide complementary information about the internal structure of materials and the shape, size, deformation and composition of quantum structures (see [4–7]). With the development of scattering theory for rough interfaces in multilayers, the grazing-angle x-ray scattering method has become a powerful non-destructive technique for probing buried interface structures with atomic resolution.

The silicon high-quality crystalline layers and SiGe alloys are promising materials for realizing quantum dot structures for x-ray terabyte storage applications, since they can readily

be implemented within existing Si technology. In the general case the procedure of digital data read-out from the X-ROM can be performed by using the principles of x-ray optics, as well as on the basis of the principles of x-ray diffraction optics. We consider in this paper a data read-out procedure based on the grazing-angle incidence x-ray backscattering diffraction (GIXB) technique, which is used under conditions of specular vacuum wave suppression. The case of ultrahigh-density digital data read-out via the normal incidence x-ray backscattering diffraction (NIXB) technique will be reported in a forthcoming paper.

## 2. Limits of the surface data density, single-bit domain area and linear size

Three-dimensional optical storage (3D storage) opens up the third dimension to increase the capacity of storage media. In principle, a volume element with the dimensions of the wavelength should suffice to store one bit, so holograms can potentially store data at a volumetric density of one bit per cubic wavelength volume of the recording medium (e.g. see [9–11]). Thus, in volumetric data storage the limit of the digital data density  $\rho_{\text{vol}}(\lambda)$  is inversely proportional to the cube of the wavelength  $\lambda$ . For a typical laser wavelength of 650 nm or so, this density corresponds to one terabyte (TB) per cubic inch or more. However, no laboratory demonstration of volumetric storage to date has got closer than approximately 1% of the volumetric density limit to one TB per cubic inch in the case of optical wavelengths.

In surface data storage, i.e. in two-dimensional data storage (2D storage) techniques, the limit of the digital data density  $\rho_{\text{sur}}(\lambda)$  is inversely proportional to the square of the wavelength  $\lambda$  (e.g. see [12]). If the x-radiation used in an X-ROM data handling system has the wavelength  $\lambda_1 \approx 0.1$  nm and the optical laser wavelength used in the DVD read-out system has e.g. the wavelength  $\lambda_2 \approx 650$  nm, then the following equations give the ratio of limits of the X-ROM and the DVD digital data surface densities:

$$\rho_{\text{sur}}(\lambda_1)/\rho_{\text{sur}}(\lambda_2) = (\lambda_2/\lambda_1)^2 = 4.225 \times 10^7. \quad (1)$$

So, further increase in two-dimensional data storage (2D storage) capacity of the digital information carriers used in optical data handling requires a technology based on a nanometre or even ångström wavelength radiation, i.e. on the x-ray wavelength. On the other hand, it is necessary to reduce the limit of surface area  $S_{\text{bit}}$  per bit of information to less than 73.3 (nm<sup>2</sup>/bit) for the purpose of increasing the digital data density of the storage medium to one TB per square inch as follows:

$$S_{\text{bit}} \leq \text{in}^2/\text{TB} = (6.4516 \times 10^{14} \text{ nm}^2)/(2^{43} \text{ bit}) \approx 73.3 \text{ nm}^2/\text{bit}. \quad (2)$$

Consequently, the following relation gives the limit of linear size  $L_{\text{bit}}$  of the X-ROM domain with a square section, which corresponds to single-bit data in the case considered, of surface data density of one TB per square inch:

$$L_{\text{bit}} = \sqrt{S_{\text{bit}}/\text{bit}} \leq 8.6 \text{ nm/bit}. \quad (3)$$

The conditions (2) and (3) determine the limitations and the requirements for surface data storage media with terabyte-scale

data density, as well as the requirements for the ultrahigh-density data recording procedure and facilities. With existing technologies, the X-ROM can be fabricated with a minimum domain linear size of about 20 nm. Taking into account (3), one may note that the digital data density of the proposed 2D storage X-ROM, with the above-mentioned linear size of single-bit domains, is two orders of magnitude higher than the volumetric data density actually achieved for the optical 3D storage medium.

### 3. Data recording and reading procedures based on x-ray diffraction optics

New generation facilities will produce x-ray beams with peak brilliance some orders of magnitude greater than what is currently available from today's synchrotron sources, and pulse durations from 100 fs to less than 1 fs. The wavelengths produced will range from 0.3 to 100 nm in the fundamental, with substantial power in the x-ray third-harmonic at 0.1 nm.

#### 3.1. Ultrahigh-density digital data recording procedure

The information transfer process, i.e. the digital data recording in the X-ROM case considered, can be viewed as the production of ultrahigh-density subsurface nanosized amorphous speckles (amorphous domains) in an x-ray optical data storage crystalline wafer.

One way to make amorphous domains is by melting and quenching nanosized domains of the sample while keeping some atoms constrained to their crystal lattice positions. Production of amorphous speckles can be performed by a pulsed laser melting method, e.g. by irradiation of supercooled high-quality crystalline storage material with in-focus femtosecond high-fluence laser pulses from a free-electron laser at extreme ultraviolet or x-ray wavelengths. However, the amorphous–crystal interfaces produced between the newly formed amorphous domains and the surrounding crystalline phase material move with each atomic rearrangement. When the subsurface two-phase structure is heated without further quenching up to the activation internal energy, which is the height of the potential energy barrier to migration, the mobility of the atoms in the amorphous phase increases sufficiently that they can hop over this energy barrier and transform into lower-energy crystalline structure phase. The crystal grows epitaxially directly from the solid amorphous phase to the solid crystal phase. The process, by which the interface moves as the amorphous atoms rearrange themselves to move into crystalline positions, is called solid phase epitaxial growth (SPEG; e.g. see [13, 14]). The growth process occurs entirely at the existing interface without the nucleation of any new crystal grains in the middle of the amorphous phase. It produces an extremely high-quality crystal growing without defects from the highly disordered amorphous phase. SPEG activation energy is over several hundred degrees Celsius for silicon and for germanium amorphous–crystal interfaces. The SPEG procedure can be used to erase digital information from the proposed storage media by the recrystallization of nanosized amorphous domains. After application of the SPEG procedure the above-mentioned x-ray optical data storage

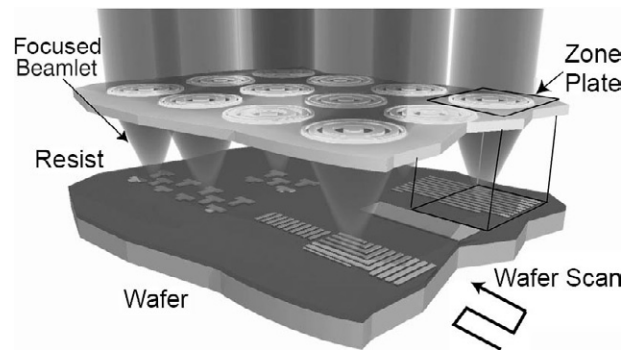


**Figure 1.** Data recording scheme, in which the maskless zone-plate-array lithography (ZPAL) technique is applied. ZPAL uses: a narrow bandwidth source, an array of diffractive lenses (e.g., Fresnel zone plates) that focuses an array of on-axis spots on the surface of a wafer coated with photosensitive material (photoresist) and a scanning stage for printing arbitrary patterns within a photoresist without a mask (e.g. see [15–24]). The recorded pattern is developed and fixed. Depending on the nature of the photoresist, the illuminated areas are removed (positive resist) or conserved (negative resist). As a result, the desired pattern is converted into a variation of the photoresist's profile height. This profile is transferred into the wafer after the chemical etching.

crystalline wafer becomes ready for further recording of information.

Another way to make nanosized amorphous domains is by technology based on x-ray nanolithography. An ultrahigh-density data recording procedure can be performed via well known maskless zone-plate-array lithography (ZPAL). A scheme of ZPAL is presented in figure 1. ZPAL uses a narrow bandwidth source, an array of diffractive lenses (e.g., Fresnel zone plates) that focuses an array of on-axis spots on the surface of a substrate coated with photosensitive material (photoresist), a multiplexing device capable of controlling the illumination of each zone plate in the array and a scanning stage, to print arbitrary patterns within a photoresist without a mask (e.g. see [15–24]). Similarly to a photograph, the recorded pattern is developed and fixed. Depending on the nature of the photoresist, the illuminated areas are removed (positive resist) or conserved (negative resist). As a result, the desired pattern is converted into a variation of the photoresist's profile height. This profile is transferred into the substrate after chemically etching the unwanted material away. The final steps of this technology are the epitaxial deposition of the x-ray high-reflectivity material inside the substrate profile windows and further stripping of the underlayer photoresist. An X-ROM prepared in such a way is a read-only x-ray optical data storage medium.

One must use the shorter wavelengths to achieve higher resolution, as was mentioned in the introduction, so, in the case of x-ray wavelengths, the anticipated resolution depends on how fine the zone plates can be made. With existing techniques, zone plates can be fabricated with minimum zone widths of about 20 nm. The massively parallel nature of the zone-plate array allows for large-area patterning much faster than is possible with a single electron beam. The light intensity of each spot is controlled by one element on a spatial light modulator (SLM). The substrate is scanned on an ultrahigh-precision stage while the elements of the SLM

are appropriately controlled, resulting in patterns of arbitrary geometry being written in a ‘dot-matrix’ fashion, with the individual beams multiplexed by an array of micromechanical shutters located upstream of the zone-plate array (e.g. see figure 1 in [15]). In ZPAL, the rate of information transfer is the product of the number of zone plates in the array and the switching speed of the SLM. The current SLM has 1088 switching elements and can operate at 0.5 MHz. With that switching speed, 1000 zone plates and eight bits per pixel (for ‘grey toning’), the information transfer rate is  $4 \times 10^9$  bits  $s^{-1}$ . The SLM can be modified to operate up to  $\sim 5$  MHz. A SLM of 5000 elements illuminating 5000 zone plates, with eight bits per pixel would result in an information transfer rate of  $2 \times 10^{11}$ , or several wafers per hour (e.g. see [23, 24]). ZPAL has already been demonstrated at blue and ultraviolet (UV) wavelengths.

### 3.2. Ultrahigh-density digital data read-out procedure

One of the powerful non-destructive experimental methods for structural investigations of single crystals and nanoscale crystalline materials is the method based on dynamical diffraction of the x-rays (e.g. see [4–7]). Grazing-angle incidence x-ray diffraction (GIXD) is a powerful non-destructive technique for investigating structural properties of surfaces, because x-rays penetrate only several hundred ångströms into the sample due to the total reflection effect. The generalized grazing-angle incidence x-ray diffraction technique has been developed in [25, 26] to investigate the structures of InAs quantum dots grown on Si(001) substrates by molecular beam epitaxy (MBE). The diameters of the InAs dots ranged from 20 to 50 nm and the average was 37 nm. Grazing-angle incidence x-ray backscattering diffraction (GIXB) is dynamical Bragg diffraction in conditions of x-ray total external reflection and can be realized only if the Bragg angle  $\theta_B$  is close to  $90^\circ$ , i.e. if the condition  $\lambda \approx 2d_{hkl}$  is met, where  $\lambda$  is the wavelength of the incident radiation,  $d_{hkl}$  is the space period of the diffracting lattice planes ( $hkl$ ) (see [27–29]).

The procedure of data reading from the nanocrystalline semiconductor X-ROM can be performed using the GIXB technique (the scheme of the coplanar GIXB configuration is presented in figure 2), under conditions of specular beam suppression (see [2, 3]). The ultrahigh-density digital information carrier used in the proposed x-ray optical data handling system, as well as the grazing-angle incident x-ray microbeam, are fixed, unlike in the conventional optical memory data read-out system. Note that under the conditions of the reflected wave suppression mode, the specular wave (unlike in other existing x-ray diffraction methods) practically carries information only about amorphous (i.e. non-diffracting) subsurface reflectors.

## 4. X-ROM polarizability model and the waves propagating in vacuum

The reciprocal vector of the set of diffracting lattice planes ( $hkl$ ) of the X-ROM backscattering crystalline elements is parallel to the  $Ox$ -axis direction according to the scheme of the coplanar GIXB configuration presented in figure 2. The polarizability  $\chi(x)$  of the set of diffracting lattice planes ( $hkl$ )

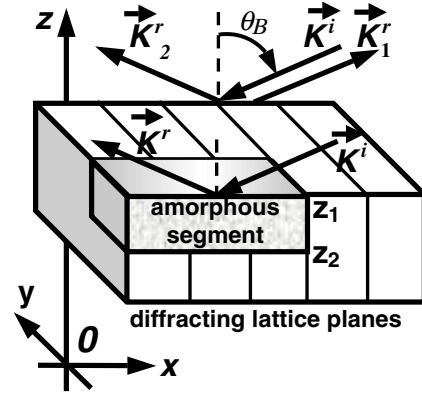


**Figure 2.** Data read-out scheme and two-segment element of the X-ROM.  $T = z_1 - z_2$  is the thickness of the amorphous component,  $\mathbf{K}^i$  and  $\mathbf{K}^r$  are the wavevectors of the incident x-ray microbeam and the specular wave reflected from the amorphous component respectively. The x-ray microbeam is back-diffracted by the crystalline segment of the X-ROM element. The angle of incidence  $\theta^i$  of the microbeam satisfies the Bragg condition, i.e.  $\theta^i = \theta_B$ , where  $\theta_B$  is the Bragg angle, the  $Ox$ -axis is normal and, consequently, the  $Oy$ -axis is parallel to the diffracting lattice planes,  $\mathbf{K}_1^i$  and  $\mathbf{K}_2^i$  are the wavevectors of the vacuum backscattered wave and specular reflected wave respectively.  $\mathbf{K}_1^r = -\mathbf{K}_1^i$ ,  $\mathbf{K}_2^r = \mathbf{K}_1^i$ . The wavevector  $\mathbf{K}_2^i$  makes an angle of  $2\theta_B$  with the wavevector  $\mathbf{K}_1^i$ . In this coplanar diffraction case there are no waves travelling along the  $y$ -axis (see [2, 3, 27–29]).

of the crystalline elements can be represented by the following equation:

$$\chi(x) = \chi_0 + \chi_g \exp(i2\pi x/d_{hkl}) + \chi_{\bar{g}} \exp(-i2\pi x/d_{hkl}) \quad (4)$$

where  $\chi_0$  is the value of the polarizability averaged throughout the crystalline element’s lattice cell,  $\chi_g$  and  $\chi_{\bar{g}}$  are the Fourier coefficients, which correspond to the set of diffracting lattice planes ( $hkl$ ). Note that the model of the polarizability considered, represented by equation (4), is valid for the description of the net planes of the natural crystals, as well as of the artificial nanocrystals, epitaxial layers, multilayers, low-dimensional structures, liquid crystals and molecular and organic–inorganic hybrid nanostructures of many types of biological object etc. We consider the case where the atom arrangement in the cell is the same or very close to that of a crystal with a symmetry centre, i.e. the following condition is fulfilled:

$$|\sin(\eta_g - \omega_g)| \ll 1, \quad (5)$$

where  $\eta_g$  and  $\omega_g$  are given in the appendix, by equations (A.8) and (A.9) respectively. Equation (4) may be rewritten in the following form taking into account equations (A.14)–(A.17) and condition (5):

$$\chi(x) \cong -|\chi_{0r}| - i|\chi_{0i}| - 2[|\chi_{gr}| + i|\chi_{gi}|] \cos[2\pi(x + x_\eta)/d_{hkl}] \quad (6)$$

where  $|\chi_{0r}|$ ,  $|\chi_{0i}|$ ,  $|\chi_{gr}|$  and  $|\chi_{gi}|$  are the absolute values of the Fourier coefficients (see the appendix and [4–7]), which correspond to the set of diffracting lattice planes ( $hkl$ );  $x_\eta$  is given in the appendix, by equation (A.16).

Let the components of stationary part  $\mathbf{E}^i(\mathbf{r})$  of a  $\sigma$ -polarized incident x-ray plane wave be given by the following equations:

$$[\mathbf{E}^i(\mathbf{r})]_x = [\mathbf{E}^i(\mathbf{r})]_z = 0, \quad (7)$$

$$[\mathbf{E}^i(\mathbf{r})]_y \equiv E_y^i(x; z) = E_0^i \exp[-i2\pi K(x \sin \theta^i + z \cos \theta^i)], \quad (8)$$

where

$$K \equiv |\mathbf{K}^i| = 1/\lambda = \nu/c, \quad (9)$$

$E_0^i$ ,  $K$  and  $\nu$  are the amplitude, wavenumber and frequency of the incident x-ray wavefield  $\mathbf{E}^i(\mathbf{r})$  respectively,  $\theta^i$  is the angle of incidence of the x-ray microbeam, which the wavevector  $\mathbf{K}^i$  forms with the  $yOz$  coordinate plane,  $c$  is the velocity of light in vacuum. Then, the following equations describe the components of stationary x-ray wavefield  $\mathbf{E}(\mathbf{r})$  inside the backscattering crystal:

$$[\mathbf{E}(\mathbf{r})]_x = [\mathbf{E}(\mathbf{r})]_z = 0, \quad (10)$$

$$\left\{ \frac{\partial^2}{\partial x^2} + \frac{\partial^2}{\partial z^2} + 4\pi^2 K^2 [1 + \chi(x)] \right\} [\mathbf{E}(\mathbf{r})]_y = 0. \quad (11)$$

If the absorption is not taken into account, then the identity  $|\chi_{0i}| \equiv |\chi_{gi}| \equiv 0$  holds. In this case the solution of (11) has the following form (see [27–29]):

$$[\mathbf{E}(\mathbf{r})]_y \equiv E_y(x; z) = \int_0^\infty \{ {}^1D_\zeta(q) c e_\zeta(u, q) + {}^2D_\zeta(q) s e_\zeta(u, q) \} \times \exp[-i2\pi z \sqrt{k^2 - (2d_{hkl})^{-2} a_\zeta}] d\zeta, \quad (12)$$

where

$$u = \pi(x + x_\eta)/d_{hkl}, \quad (13)$$

$$q = (2K d_{hkl})^2 |\chi_{gr}|, \quad (14)$$

$$k = K \sqrt{1 - |\chi_{0r}|}, \quad (15)$$

$${}^2D_0(q) \equiv 0, \quad (16)$$

$c e_\zeta(u; q)$  and  $s e_\zeta(u; q)$  are the ordinary Mathieu functions of the first kind, to which the eigenvalues  $a_\zeta$  correspond (e.g. see [30–35]). According to equations (7) and (10), we suppose the fulfilment of the following relations for the  $x$  and  $z$  components of the electric strength  $\mathbf{E}^r(\mathbf{r})$  of the stationary part of the x-ray wavefield reflected from the X-ROM crystalline elements:

$$[\mathbf{E}^r(\mathbf{r})]_x \cong [\mathbf{E}^r(\mathbf{r})]_z \cong 0. \quad (17)$$

We search for the  $y$  component of the electric strength  $\mathbf{E}^r(\mathbf{r})$  in the Fourier integral form:

$$[\mathbf{E}^r(\mathbf{r})]_y \equiv E_y^r(x; y; z) \cong \int_{-\infty}^\infty E_0^r(y; K_x^r) \times \exp \left\{ -i2\pi \left[ x K_x^r - z \sqrt{K^2 - (K_x^r)^2} \right] \right\} dK_x^r. \quad (18)$$

The wavefields presented by equations (8), (12) and (18) must satisfy the following boundary conditions:

$$E_y^i(x; z_1) + E_y^r(x; z_1) - E_y(x; z_1) = 0, \quad (19)$$

$$\left\{ \frac{\partial}{\partial z} [E_y^i(x; z) + E_y^r(x; z) - E_y(x; z)] \right\} \Big|_{z=z_1} = 0, \quad (20)$$

where the plane  $z = z_1$  is the X-ROM's entrance surface. Using the orthogonality conditions of the functions involved in equations (12) and (18), the unknown weight functions  ${}^1D_\zeta(q)$ ,  ${}^2D_\zeta(q)$  and  $E_0^r(y; K_x^r)$ , which satisfy the boundary conditions (19) and (20), should be found. One obtains

the required expressions for the reflected and transmitted wavefields by the corresponding substitution of the obtained weight functions into (12) and (18).

Depending on the choice of storage media properties, as well as on the fine adjustment of the microbeam wavelength and angle of incidence, the intensity of the specular wave reflected from an amorphous element can exceed several times the intensity of the specular wave reflected from a crystalline element operating under GIXB conditions [2]. In the GIXB configuration the entire vacuum x-ray wavefield reflected from the perfect crystalline regions consists of two plane components (see [2, 3, 27–29]): vacuum back-diffracted and specular reflected waves (see figure 2). In the particular case of coplanar GIXB, the reflected x-ray wavefield  $\mathbf{E}^r(\mathbf{r})$  may be presented in the following form:

$$\begin{aligned} \mathbf{E}^r(\mathbf{r}) &\equiv \mathbf{E}^r(x; y; z; \theta_B) = \sum_{n=1}^2 \mathbf{E}_n^r(x; y; z; \theta_B; \mathbf{K}_n^r) \\ &= \sum_{n=1}^2 \{ \hat{\mathbf{x}} [\mathbf{E}_n^r(x; y; z; \theta_B; \mathbf{K}_n^r)]_x \\ &\quad + \hat{\mathbf{y}} [\mathbf{E}_n^r(x; y; z; \theta_B; \mathbf{K}_n^r)]_y \}, \end{aligned} \quad (21)$$

where the angle of incidence  $\theta^i$  satisfies the Bragg condition, i.e.  $\theta^i = \theta_B$ ,  $\mathbf{K}_1^r$  and  $\mathbf{K}_2^r$  are the wavevectors of the vacuum backscattered wave and specular reflected wave respectively (see figure 2),  $\hat{\mathbf{x}}$  and  $\hat{\mathbf{y}}$  are the unit vectors in the directions of the  $Ox$ - and  $Oy$ -axes correspondingly. In the coplanar GIXB configuration the reflected x-ray wavefield components  $[\mathbf{E}_n^r(x; y; z; \theta_B; \mathbf{K}_n^r)]_\xi$  (where  $\xi = x; y$ ) are presented in the paper [29], and also can be derived from the equations presented in appendix A of paper [2]. Absorption can be taken into account if the following substitutions are made in the equations for the reflected x-ray wavefield components presented in the paper [29]:

$$|\chi_{0r}| \rightarrow |\chi_{0r}| + i|\chi_{0i}|, \quad (22)$$

$$|\chi_{gr}| \rightarrow |\chi_{gr}| + i|\chi_{gi}|. \quad (23)$$

## 5. Specular vacuum wave suppression and enhancement phenomena

The phenomenon of suppression [2] of specular vacuum waves can be applied in the development of new optical device components operating in the GIXB configuration, particularly for the implementation of the procedure of data reading from the semiconductor X-ROM media. The proposed data read-out system detects data by measuring the changes in the x-ray microbeam intensity reflected from the semiconductor X-ROM layer in the case where the Bragg condition is satisfied for the crystalline segments of the X-ROM elements. For the given value of the wavelength  $\lambda$  of the incident x-ray plane wave, the specular beam suppression and enhancement phenomena are most clearly observable in the coplanar GIXB configuration realized as in the case of perfect single crystal, as well as in the case of crystal containing a stacking fault [2].

The images of the characteristic functions presented in figures 3(a) and (b) are graphs of the difference  $\Delta R(\theta_B) = R_2(\theta_B) - R(\theta^i)$  and the ratio  $R(\theta^i)/R_2(\theta_B)$  respectively, where

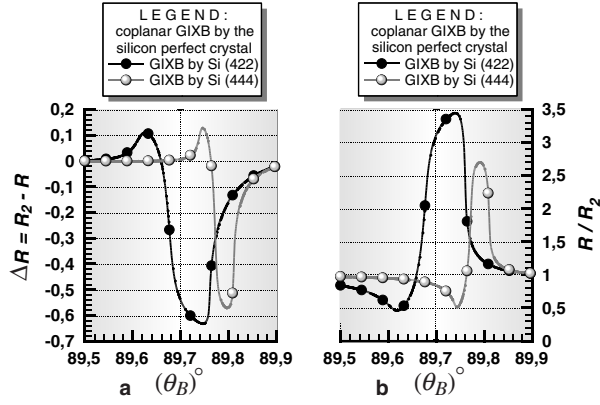


**Figure 3.** Images of the difference  $\Delta R(\theta_B) = R_2(\theta_B) - R(\theta^i)$  and the ratio  $R(\theta^i)/R_2(\theta_B)$  in the particular case of the X-ROM, which consists of a crystalline silicon wafer with subsurface amorphous nanosized silicon domains (reflecting speckles) introduced e.g. by the pulsed in-focus femtosecond laser melting method, where  $R_2(\theta_B)$  is the specular beam reflectivity coefficient when the GIXB takes place,  $R(\theta^i)$  is the specular beam reflectivity coefficient when the Bragg condition is not satisfied. The X-ROM prepared by such a method is a read-write x-ray optical data storage medium, since digital information can be erased by the recrystallization of nanosized amorphous domains, e.g. using the solid phase epitaxial growth (SPEG) procedure. After application of the SPEG procedure the crystalline wafer becomes ready for further recording of information. The curves presented correspond to x-ray backscattering diffraction by the perfect silicon crystal's two different net planes (422) and (444). The graphs relate to the particular case of the coplanar GIXB configuration when the angle of incidence  $\theta^i = \theta_B$  of the x-ray plane wave satisfies the Bragg condition: (a) images of the difference  $\Delta R(\theta_B)$  between the reflection coefficients, (b) images of the ratio  $R(\theta^i)/R_2(\theta_B)$  of the reflection coefficients.

$R_2(\theta_B)$  is the specular beam reflectivity coefficient when the coplanar GIXB takes place:

$$R_2(\theta_B) = |\mathbf{E}_0^i|^{-2} \{ |\mathbf{E}_2^r(x; z; \theta_B; \mathbf{K}_2^r)|_x|^2 + |\mathbf{E}_2^r(x; z; \theta_B; \mathbf{K}_2^r)|_y|^2 \}, \quad (24)$$

$R(\theta^i)$  is the specular beam reflectivity coefficient when the Bragg condition is not satisfied,  $\mathbf{E}_0^i$  is the amplitude of the incident x-ray plane wave. These graphs are calculated in the particular case of an X-ROM which consists of a crystalline silicon wafer with subsurface amorphous nanosized silicon domains (reflecting speckles) introduced e.g. by a pulsed in-focus femtosecond laser melting method. Digital data are encoded with certain positions of the above-mentioned amorphous nanosized silicon domains. An X-ROM prepared by such a method is a read-write x-ray optical data storage medium, since digital information can be erased by the recrystallization of nanosized amorphous domains, e.g. using the solid phase epitaxial growth (SPEG) procedure, after which the crystalline wafer becomes ready for further recording of new information. Negative values of  $\Delta R(\theta_B)$  characterize the specular beam suppression phenomenon and positive values of  $\Delta R(\theta_B)$  characterize the specular beam enhancement phenomenon. Values of the ratio  $R(\theta^i)/R_2(\theta_B)$  over unity characterize specular beam suppression and values less than unity characterize the specular beam enhancement phenomenon. The graphs

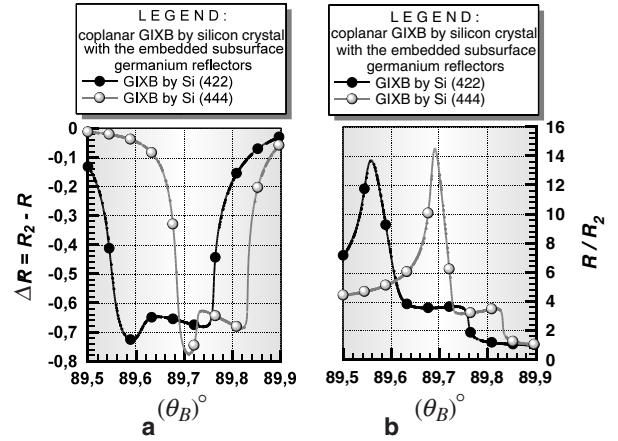


**Figure 4.** Images of the difference  $\Delta R(\theta_B) = R_2(\theta_B) - R(\theta^i)$  and the ratio  $R(\theta^i)/R_2(\theta_B)$  in the particular case of an X-ROM which consists of a crystalline silicon wafer with regularly embedded subsurface germanium domains (reflecting speckles) produced by the technology based on x-ray nanolithography, where  $R_2(\theta_B)$  is the specular beam reflectivity coefficient when GIXB by the silicon wafer takes place,  $R(\theta^i)$  is the reflectivity coefficient of the x-ray beam reflected from the non-diffracting germanium domain. Digital data are encoded with certain positions of the nanosized germanium domains. An X-ROM prepared in such a way is a read-only x-ray optical data storage medium. The curves presented correspond to x-ray backscattering diffraction by the silicon wafer's two different net planes (422) and (444). The graphs relate to the particular case of the coplanar GIXB configuration when the angle of incidence  $\theta^i = \theta_B$  of the x-ray plane wave satisfies the Bragg condition: (a) images of the difference  $\Delta R(\theta_B)$  between the reflection coefficients, (b) images of the ratio  $R(\theta^i)/R_2(\theta_B)$  of the reflection coefficients.

presented provide the possibility of choosing the Bragg angle  $\theta_B$  optimally and, consequently, also the incident radiation wavelength  $\lambda$  appropriate for the proposed digital data read-out procedure. The graphs relate to the particular case of the coplanar GIXB configuration when the angle of incidence  $\theta^i = \theta_B$  of the x-ray plane wave satisfies the Bragg condition. These graphs correspond to x-ray backscattering diffraction by the perfect silicon crystal's two different net planes (422) and (444). If the x-ray backscattering diffraction is effected by the net planes (422) of the silicon X-ROM's crystalline segments, one may conclude from figures 3(a) and (b) that the x-ray specular beam suppression phenomenon is most clearly observable at  $\theta^i = \theta_B = 89.75^\circ$ . Also, as is seen from these figures, the x-ray specular beam suppression phenomenon is most clearly observable at  $\theta^i = \theta_B = 89.79^\circ$  in the case of x-ray backscattering diffraction by the net planes (444) of the silicon X-ROM's crystalline segments.

## 6. Case when the refractive indices of the wafer and of the embedded domains are different

Images of the characteristic functions presented in figures 4(a) and (b) correspond to another particular case of an X-ROM. The digital data storage medium considered is a crystalline silicon wafer with regularly embedded subsurface germanium domains (reflecting speckles) produced e.g. via an x-ray

nanolithography technique. The function  $R_2(\theta_B)$  is the specular beam reflectivity coefficient when GIXB by the silicon wafer takes place, and the function  $R(\theta^i)$  is the reflectivity coefficient of the x-ray beam reflected from the non-diffracting germanium domain. Digital data are encoded with certain positions of the nanosized germanium domains. The X-ROM prepared in such a way is a read-only x-ray optical data storage medium. The curves presented correspond to x-ray backscattering diffraction by the silicon wafer's two different net planes (422) and (444). The graphs relate to the particular case of the coplanar GIXB configuration when angle of incidence  $\theta^i = \theta_B$  of the x-ray plane wave satisfies the Bragg condition. From figures 4(a) and (b) it follows that the x-ray specular beam suppression phenomenon is most clearly observable at  $\theta^i = \theta_B = 89.73^\circ$  in the case of x-ray backscattering diffraction by the net planes (422) of the silicon X-ROM's crystalline segments. Also, as is seen from these figures, the x-ray specular beam suppression phenomenon is most clearly observable at  $\theta^i = \theta_B = 89.82^\circ$  in the case of x-ray backscattering diffraction by the net planes (444) of the silicon X-ROM's crystalline segments.

However, as is seen from figure 4(a), an additional local minimum useful for the data read-out procedure is situated either at  $\theta^i = \theta_B = 89.59^\circ$  or at  $\theta^i = \theta_B = 89.82^\circ$  depending on the choice of net plane from which the x-ray backscattering diffraction takes place. The appearance of this new local minimum point is raised solely by the difference in refractive index of germanium and silicon. Analogously, each of the curves presented in the figure 4(b) has two local maxima, unlike the images presented in the figure 3(b). Thus, each of the curves presented in figures 4(a), (b) has two extremum points, one of which appears due to GIXB under conditions of specular vacuum wave suppression, the appearance of the other one being governed by the difference in refractive index of the wafer material and the embedded domains.

As was mentioned in section 3, the positions of the ultrahigh-density digital information carrier and of the grazing-angle incident x-ray microbeam are fixed in the proposed X-ROM based data handling system, unlike in the conventional optical memory data read-out systems. Such a grazing-angle incidence x-ray diffraction configuration allows the simultaneous handling of data from a very large area and, consequently, the data read-out speed is much faster than in the optical data read-out systems. The procedure of digital data reading from the proposed X-ROM would be very effective if it was performed by a fast charge-coupled device (fast CCD) based x-ray multi-channel area detector, whose array of detecting pixels is of the same size or larger than the array of stored data pixels of the whole X-ROM.

## 7. Conclusions

Ultrahigh-density semiconductor x-ray optical memory (X-ROM) is proposed (also see [2, 3]). The X-ROM considered in this paper is an information carrier destined for a digital data reading procedure based on x-ray diffraction optics.

The data recording procedure can e.g. be performed by the in-focus femtosecond high-fluence laser pulses of a free-electron laser at extreme ultraviolet or x-ray wavelengths. This method makes amorphous domains by melting and quenching

nanosized domains of the sample while keeping some atoms constrained to their crystal lattice positions. If the subsurface two-phase structure is heated without further quenching up to the activation internal energy, then the mobility of the atoms in the amorphous phase increases sufficiently that they can hop over the potential energy barrier and effect a transformation into the lower-energy crystalline structure phase. This can be used to erase digital information from the proposed storage media, by the recrystallization of nanosized amorphous domains. Application of such a heating procedure makes the crystalline wafer ready for further recording of the information. Another way to make nanosized amorphous domains is the well known ZPAL technique (see figure 1 and references [15–24]).

The data reading from a nanocrystalline semiconductor X-ROM can e.g. be performed using the GIXB technique (see figure 2), under conditions of specular beam suppression. The x-ray source for the data read-out procedure could e.g. be a Rigaku 18 kW copper rotating anode generator. Such x-ray sources could easily be utilized in state, public service and educational institutions, libraries, laboratories etc. The required parts of the information stored in the X-ROM could be spread to personal users via a 'Professional Disk for Data', which employs a blue laser with a wavelength of just 405 nm, enabling recording up to 23 GB on one side of a disk.

The differences  $\Delta R(\theta_B) = R_2(\theta_B) - R(\theta^i)$  between the specular beam reflectivity coefficients, as well as the ratio  $R(\theta^i)/R_2(\theta_B)$ , characterize the specular vacuum wave suppression and enhancement phenomena. Images of the difference  $\Delta R(\theta_B)$  and of the ratio  $R(\theta^i)/R_2(\theta_B)$  are presented in figures 3(a) and (b) respectively. These images correspond to coplanar GIXB by the diffracting lattice planes (422) and (444) of the silicon crystal with non-diffracting subsurface inclusions when the angle of incidence  $\theta^i = \theta_B$  of the plane wave satisfies the Bragg condition.

Images of the difference  $\Delta R(\theta_B) = R_2(\theta_B) - R(\theta^i)$  and the ratio  $R(\theta^i)/R_2(\theta_B)$  in the particular case of an X-ROM which consists of a crystalline silicon wafer with regularly embedded subsurface germanium domains (reflecting speckles) are presented in figures 4(a) and (b) respectively, where the coefficient  $R_2(\theta_B)$  is the same as for figures 3(a) and (b). An X-ROM prepared in such a way is a read-only x-ray optical data storage medium. In this case the coefficient  $R(\theta^i)$  is the reflectivity coefficient of the x-ray beam reflected from the non-diffracting germanium domain. The curves presented correspond to x-ray back-diffraction by the silicon wafer's two different net planes (422) and (444). The graphs relate to the particular case of a coplanar GIXB configuration when the angle of incidence  $\theta^i = \theta_B$  of the x-ray plane wave satisfies the Bragg condition.

Each of the curves presented in figures 4(a) and (b) has two local extremum points. One of these points appears due to GIXB under conditions of specular vacuum wave suppression. The appearance of the other one is governed by the difference in refractive index of the wafer material and the embedded domains. This additional point can also be utilized in the proposed data read-out technique (see the detailed consideration in our forthcoming paper).

In the proposed data read-out system the positions of the ultrahigh-density digital information carrier and of the

grazing-angle incident x-ray microbeam are fixed, unlike in the conventional optical data read-out systems. The grazing-angle incidence x-ray diffraction configuration allows simultaneous data read-out from practically all of the area of the ultrahigh-density x-ray optical data carrier.

### Appendix. Complex-valued Fourier coefficients of the polarizability model

Deviation from ideal elastic scattering, i.e. the presence of absorption, is described formally by the complex-valued coefficients (e.g. see [4–7]):

$$\chi_0 = \chi_{0r} + i\chi_{0i}, \quad (\text{A.1})$$

$$\chi_g = \chi_{gr} + i\chi_{gi}, \quad (\text{A.2})$$

$$\chi_{\bar{g}} = \chi_{\bar{g}r} + i\chi_{\bar{g}i}. \quad (\text{A.3})$$

The complex nature of  $\chi_0$  depends upon the nature of the atoms that produce the absorption, and  $\chi_{0r}$  and  $\chi_{0i}$  are real quantities. Unlike  $\chi_{0r}$  and  $\chi_{0i}$ , however,  $\chi_{gr}$  and  $\chi_{gi}$  depend not only on the nature of the atoms but also on their arrangement in the cell, and may be complex if the crystal has no symmetry centre. However,  $\chi_{gr}$ ,  $\chi_{\bar{g}r}$  and  $\chi_{gi}$ ,  $\chi_{\bar{g}i}$  are pairs of conjugate complex quantities (e.g. see [4–7]):

$$\chi_{gr} = |\chi_{gr}| \exp(i\eta_g), \quad (\text{A.4})$$

$$\chi_{\bar{g}r} = |\chi_{gr}| \exp(-i\eta_g), \quad (\text{A.5})$$

$$\chi_{gi} = |\chi_{gi}| \exp(i\omega_g), \quad (\text{A.6})$$

$$\chi_{\bar{g}i} = |\chi_{gi}| \exp(-i\omega_g), \quad (\text{A.7})$$

where

$$-\pi \leq \eta_g \leq \pi, \quad (\text{A.8})$$

$$-\pi \leq \omega_g \leq \pi. \quad (\text{A.9})$$

Coefficients  $\chi_{gr}$ ,  $\chi_{\bar{g}r}$ ,  $\chi_{gi}$  and  $\chi_{\bar{g}i}$  are real quantities if the crystal has a symmetry centre; therefore in such cases of atomic arrangement in the crystal's unit cell, the quantities  $\eta_g$  and  $\omega_g$  are either 0 or  $\pi$ . Equations (A.1)–(A.3) may be rewritten in the following form:

$$\chi_0 = -|\chi_{0r}| - i|\chi_{0i}|, \quad (\text{A.10})$$

$$\chi_g = |\chi_{gr}| \exp(i\eta_g) + i|\chi_{gi}| \exp(i\omega_g), \quad (\text{A.11})$$

$$\chi_{\bar{g}} = |\chi_{gr}| \exp(-i\eta_g) + i|\chi_{gi}| \exp(-i\omega_g). \quad (\text{A.12})$$

Taking into account equations (A.10)–(A.12), equation (4) may be rewritten finally in the form below:

$$\chi(x) = \chi_r(x) + i\chi_i(x), \quad (\text{A.13})$$

where

$$\chi_r(x) = -|\chi_{0r}| - 2|\chi_{gr}| \cos[2\pi(x + x_\eta)/d_{hkl}], \quad (\text{A.14})$$

$$\chi_i(x) = -|\chi_{0i}| - 2|\chi_{gi}| \cos[2\pi(x + x_\omega)/d_{hkl}], \quad (\text{A.15})$$

$$x_\eta = (2\pi)^{-1}(\eta_g - \pi)d_{hkl}, \quad (\text{A.16})$$

$$x_\omega = (2\pi)^{-1}(\omega_g - \pi)d_{hkl}. \quad (\text{A.17})$$

### References

- [1] Cho Y, Fujimoto K, Hiranaga Y, Wagatsuma Y, Onoe A, Terabe K and Kitamura K 2003 Terabit inch<sup>-2</sup> ferroelectric data storage using scanning nonlinear dielectric microscopy nanodomain engineering system *Nanotechnology* **14** 637–42
- [2] Bezirganyan H P, Bezirganyan H H Jr, Bezirganyan S E and Bezirganyan P H Jr 2004 Specular beam suppression and enhancement phenomena in the case of grazing-angle incidence x-rays backdiffraction by the crystal with stacking fault *Opt. Commun.* **238** 13–28
- [3] Bezirganyan H P, Bezirganyan H H Jr, Bezirganyan S E and Bezirganyan P H Jr 2004 Ultrahigh-density semiconductor data storage media useful for data readout by x-ray microbeam *Book of Abstracts of III International Optical Congress 'Optics-XXI Century' and III International Conference 'Basic Problems of Optics', Topical Meeting on Optoinformatics (Saint-Petersburg, Russia, Oct. 2004)* p 48
- [4] James R W 1967 *The Optical Principles of the Diffraction of X-rays* (Ithaca, NY: Cornell University Press)
- [5] Azaroff L V, Kaplow R, Kato N, Weiss R J, Wilson A J C and Young R A 1974 X-ray diffraction *International Series in Pure and Applied Physics* ed J L Farnsworth and J W Bradley (New York: McGraw-Hill)
- [6] Pinsker Z G 1981 *Dynamical Scattering of X-Rays in Crystals* (Berlin: Springer)
- [7] Authier A 2001 *Dynamical Theory of X-Ray Diffraction* (Oxford: Oxford University Press)
- [8] Lagomarsino S, Sedola A, Di Fonzo S, Jark W, Mocella V, Pelka J and Riekel C 2002 Advances in microdiffraction with x-ray waveguide *Cryst. Res. Technol.* **37** 757–68
- [9] Burr G W 2003 Three-dimensional optical storage *Proc. SPIE* **5225** 172–83
- [10] Burr G W 2003 Volumetric storage *Encyclopedia of Optical Engineering* ed R B Johnson and R G Driggers (New York: Dekker)
- [11] Burr G W 2003 Holographic storage *Encyclopedia of Optical Engineering* ed R B Johnson and R G Driggers (New York: Dekker)
- [12] Mansuripur M 1995 *The Physical Principles of Magneto-Optical Recording* (Cambridge: Cambridge University Press)
- [13] Olson G L and Roth J A 1994 Solid phase epitaxy *Handbook of Crystal Growth* vol 3, ed D T J Hurler (Amsterdam: North-Holland-Elsevier) chapter 7
- [14] Barvosa-Carter W and Aziz M J 2001 Time-resolved measurements of stress effects on solid-phase epitaxy of intrinsic and doped Si *Appl. Phys. Lett.* **79** 356–8
- [15] Smith H I 1996 A proposal for maskless, zone-plate-array nanolithography *J. Vac. Sci. Technol. B* **14** 4318–22
- [16] Smith H I, Carter D J D, Meinhold M, Moon E E, Lim M H, Ferrera J, Walsh M, Gil D and Menon R 2000 Soft x-rays for deep sub-100 nm lithography, with and without masks *Microelectron. Eng.* **53** 77–84
- [17] Gil D, Menon R, Tang X, Smith H I and Carter D J D 2002 Parallel maskless optical lithography for prototyping, low-volume production, and research *J. Vac. Sci. Technol. B* **20** 2597–601
- [18] Di Fabrizio E M 2003 Nano-optical elements fabricated by x-ray lithography *Proc. SPIE* **5225** 213–9
- [19] Gil D, Menon R and Smith H I 2003 The case for diffractive optics in maskless lithography *J. Vac. Sci. Technol. B* **21** 2810–4
- [20] Gil D, Menon R and Smith H I 2004 The promise of diffractive optics in maskless lithography *Microelectron. Eng.* **73/74** 35–41
- [21] Menon R, Patel A, Moon E E and Smith H I 2004 Alpha-prototype system for zone-plate-array lithography *J. Vac. Sci. Technol. B* **22** 3032–7

- [22] Menon R, Moon E E, Mondol M K, Castaño F J and Smith H I 2004 Scanning-spatial-phase alignment for zone-plate-array lithography *J. Vac. Sci. Technol. B* **22** 3082–5
- [23] Menon R, Patel A, Gil D and Smith H I 2005 Maskless lithography *Mater. Today* **2** 26–33
- [24] Payne A, DeGroot W, Monteverde R and Amm D 2004 Enabling high-data-rate imaging applications with grating light valve technology *Proc. SPIE* **5348** 76–88
- [25] Uragami T, Acosta A S, Fujioka H, Mano T, Ohta J, Ofuchi H, Oshima M, Takagi Y, Kimura M and Suzuki T 2002 Characterization of strain distribution in quantum dots by x-ray diffraction *J. Cryst. Growth* **234** 197–201
- [26] Kimura M, Acosta A, Fujioka H and Oshima M 2003 Generalized grazing-incidence-angle x-ray scattering analysis of quantum dots *J. Appl. Phys.* **93** 2034–40
- [27] Bezirganyan H P and Bezirganyan P H 1988 Solution of the two-dimensional stationary Schroedinger equation with cosine-like coefficient (in view of x-ray diffraction) *Phys. Status Solidi a* **105** 345–55
- [28] Bezirganyan H P 1988 X-ray reflection from and transmission through a plane-parallel dielectric plate with cosine-like polarizability (symmetrical Laue case;  $\theta_B \approx \pi/2$ ) *Phys. Status Solidi a* **109** 101–10
- [29] Bezirganyan H P, Bezirganyan S E, Bezirganyan H H Jr and Bezirganyan P H Jr 2002 Backdiffraction configuration for x-ray standing wave formed just above the surface of the crystal containing a stacking fault *Malaysian J. Sci. A* **21** 31–40 (Special issue)
- [30] Mathieu E 1868 Memoire sur le Mouvement Vibratoire d'une Membrane de Forme Elliptique *J. Math. Pure Appl. (J. de Liouville)* **13** 137–203
- [31] McLachlan N W 1947 *Theory and Application of Mathieu Functions* (Oxford: Oxford University Press) (1964; New York: Dover)
- [32] Bateman H and Erdelyi A 1953 *Higher Transcendental Functions* vol 3 (New York: McGraw-Hill)
- [33] Whittaker E T and Watson G N 1965 *A Course of Modern Analysis* (New York: Cambridge University Press) chapter XXIII
- [34] Abramowitz M and Stegun I A (ed) 1972 *Handbook of Mathematical Functions (National Bureau of Standards Applied Mathematics Series vol 55)* (New York: Dover) pp 721–46
- [35] Meixner J, Schaefer F W and Wolf G 1980 *Mathieu Functions and Spheroidal Functions and their Mathematical Foundations* (Berlin: Springer)